Available online at www.sciencedirect.com
SciVerse ScienceDirect
Physics Procedia 32 (2012) 614 – 622
Physics Procedia

18th International Vacuum Congress, Beijing of P. R. China, August 2010

Numerical research about the internal flow of steam-jet vacuum pump: evaluation of turbulence models and determination of the shock-mixing layer

Jingliang Dong[a], Xiaodong Wang[a*], Jiyuan Tu[b]

[a]*School of Mechanical Engineering & Automation, Northeastern University, Shenyang 110819, P. R. China*
[b]*School of Aerospace, Mechanical and Manufacturing Engineering, RMIT University, Victoria 3083, Australia*

Abstract

Steam-jet vacuum pump is widely used in a range of applications. This paper evaluated the performance of four well-known turbulence models for predicting and understanding the internal flow of a steam-jet vacuum pump first. With the help of a commercial computational fluid dynamics (CFD) code ANSYS-Fluent 6.3, the simulation results obtained from the concerned turbulence models were compared with experimental values, the k-omega-SST model was chosen as a tool model for carrying out numerical simulations. Then, based on the simulation results obtained from specific operating conditions, a method for locating the shock-mixing layer was put forward. The shape of the shock-mixing layer shows that the secondary steam does not mix with the primary steam immediately after being induced into the mixing chamber of the pump; actually, they maintain their independence till the shocking position instead. After the shock happens, the shock-mixing layer disappear, the two fluid in the pump begin to mix with each other and discharge to the next stage with almost the same state. Based on the shape of the shock-mixing layer and the supersonic region of the secondary steam, a detailed analysis for the flow duct of the secondary steam was carried out. It is found that the throat of the secondary steam flow duct plays a crucial role in maintaining a stable operating state and the length of the throat reflects the back pressure endurance for the pump.

PACS: 47.27.E-, 42.27.wj
Keywords: Steam-jet vacuum pump; CFD; turbulence model; shock-mixing layer

1. Introduction

Steam-jet vacuum pump is one of the most important equipments widely used in chemistry, petroleum, metallurgy, refrigeration and food industry to obtain a vacuum environment for various special techniques with very little electrical or mechanical energy consumption. Its features and applications have been widely discussed by Huang et al. [1] and Eames et al. [2].

A steam-jet vacuum pump is composed of a Laval nozzle, a mixing chamber, throat and a diffuser as shown in Fig. 1 [3], velocity and pressure profiles along the pump are also illustrated in the same diagram. The steam with

* Corresponding author. Tel.: +86-24-8368 7618; fax: +86-24-8368 0459.
E-mail address: xdwang@mail.neu.edu.cn

 doi:10.1016/j.phpro.2012.03.608

high total energy is called the primary steam or motive steam while the other, with the lower total energy, is called the secondary steam or induced steam. The primary steam with high pressure expands through the Laval nozzle and reaches to supersonic speed and produces a low pressure (vacuum) region at the outlet of the Laval nozzle. By an entrainment-induced effect, the secondary steam is draw into the mixing chamber and accelerated. This process is accompanied by energy and momentum exchanging between the primary and secondary steam. A normal shock wave is induced in the throat and the speed of the mixing fluid suddenly drops to subsonic value. Further compression is achieved when the mixed fluid passes through the diffuser.

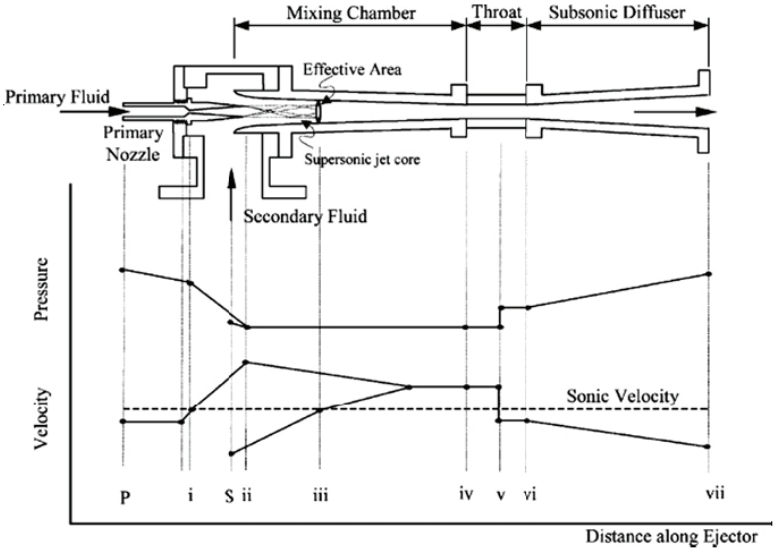

Fig.1: A typical steam-jet vacuum pump and its flow characteristics

Many theoretical [4-6] and experimental [7] studies were performed in order to understand not only the fundamental mechanisms in terms of fluid dynamics and heat transfer, but also pump operational behavior. Although these studies made considerable and remarkable progress for the general understanding of steam-jet vacuum pump, they still unable to reproduce the flow physics locally along the pump correctly, some very fundamental problems have yet to be overcome, especially the modeling and understanding of shock-mixing layer interaction as well as its influence on the mixing process and recompression rate [8] which will allow a more reliable and accurate design, in terms of geometry and operation conditions. Computational fluid dynamics (CFD) is a good choice as a research tool to investigate and predict the complicated flow in a steam-jet vacuum pump, and it is expected to provide a good understanding of local phenomena at a reasonable cost. Numerous CFD studies about this field have been achieved since the 1990s [9-11], however none of them has made effort to provide a reasonable and feasible approach to determine the shape and location of the shock-mixing layer. So our primary interest in this paper is the determination of the shock-mixing layer and the influence of different operating parameters on it.

2. Mathematical Models

2.1. Governing equations

The flow in steam-jet vacuum pump is governed by the compressible steady-state axisymmetric form of the fluid flow conservation equations. For variable density flows, the Favre averaged Navier-Stokes equations are more suitable and will be used in this work. The total energy equation including viscous dissipation is also included and coupled to the set with the perfect gas law. The thermodynamics and transport properties for steam are held constant; their influence was not found to be significant with the validation runs. The governing equations can therefore be written in their compact Cartesian form:

The continuity equation:

$$\partial\rho/\partial t + \partial(\rho u_i)/\partial x_i = 0 \tag{1}$$

The momentum equation:

$$\partial(\rho u_i)/\partial t + \partial(\rho u_i u_j)/\partial x_j = -\partial P/\partial x_i + \partial \tau_{ij}/\partial x_j \tag{2}$$

The energy equation:

$$\partial(\rho E)/\partial t + \partial(u_i(\rho E + P))/\partial x_i = \vec{\nabla}(\alpha_{\text{eff}}\partial T/\partial x_i) + \vec{\nabla}(u_j \tau_{ij}) \tag{3}$$

where

$$\tau_{ij} = \mu_{\text{eff}}(\partial u_i/\partial x_j + \partial u_j/\partial x_i) - \frac{2}{3}\mu_{\text{eff}}(\partial u_k/\partial x_k)\delta_{ij} \tag{4}$$

with

$$\rho = P/(RT) \tag{5}$$

2.2. Turbulence modeling

Most of the turbulence models used in this paper rely on the Boussinesq hypothesis. It means that they are based on an eddy viscosity assumption, which makes the Reynolds stress tensor coming from equation averaging, to be proportional to the mean deformation rate tensor:

$$-\rho\overline{u_i' u_j'} = \mu_t(\partial u_i/\partial x_j + \partial u_j/\partial x_i) - \frac{2}{3}(\rho k + \mu_t \partial u_i/\partial x_i)\delta_{ij} \tag{6}$$

The advantage of this approach is the relatively low computational cost associated with the determination of the turbulent viscosity, and suitable for industrial application. However, the main drawback of this hypothesis is the assumption that the turbulence is isotropic. The k-epsilon, realizable-k-epsilon and k-omega models are based on this hypothesis. Only the Reynolds stress model (RSM) does not rely on this assumption, but the associated CPU cost may be relatively high [12]. Based on our simulation results, the k-omega-SST model appears to be the most accurate model for ejector analysis. It is therefore described in more detail as below. The description of the other turbulence models listed can be found in ANSYS Fluent Theory Guide [13].

The equation for k is:

$$\frac{\partial}{\partial t}(\rho k) + \frac{\partial}{\partial x_i}(\rho k u_i) = \frac{\partial}{\partial x_j}\left(\Gamma_k \frac{\partial k}{\partial x_j}\right) + G_k - Y_k + S_k \tag{7}$$

The equation for ω is:

$$\frac{\partial}{\partial t}(\rho \omega) + \frac{\partial}{\partial x_i}(\rho \omega u_i) = \frac{\partial}{\partial x_j}\left(\Gamma_\omega \frac{\partial \omega}{\partial x_j}\right) + G_\omega - Y_\omega + D_\omega + S_\omega \tag{8}$$

In these equations, G_k represents the generation of turbulence kinetic energy due to mean velocity gradients, G_ω represents the generation of ω, Γ_k and Γ_ω represent the effective diffusivity of k and ω, respectively, Y_k and Y_ω represent the dissipation of k and ω due to turbulence, D_ω represents the cross-diffusion term. Details on the expressions of these terms can be found in [14]. In addition, the eddy viscosity is redefined so as to take into account the transport of the principal turbulent shear stress [14].

2.3. Compressibility corrections

For k-omega models, it is included in Y_ω and it consists in replacing M_t by a compressibility function $F(M_t)$:

$$F(M_t) = \begin{cases} 0 & M_t \le M_{t0} \\ M_t^2 - M_{t0}^2 & M_t > M_{t0} \end{cases} \tag{9}$$

where

$$M_t^2 = 2k/a^2 \tag{10}$$

$$M_{t0} = 0.25 \tag{11}$$

$$a = \sqrt{\gamma RT} \tag{12}$$

The advantage of this compressibility function is that it does not take effect everywhere in the flow field, but just in some places where compressibility becomes important.

3. Numerical simulations

The geometric parameters of the steam-jet vacuum pump experiment model set-up by Sriveerakul are summarized in Table 1 [15]. The primary and secondary fluids are steam and the parameters are summarized in Table 2. The study by Pianthong, Seehanam was shown that the simulation results for flow properties by the 2D axis symmetric model (ASXM) and three dimensional model (3D) were very close [16], it means that the ASXM is good enough to get accurate results. ASXM is adopted in present study to simulate and analyze the flow in steam-jet vacuum pump which would save lots of computing cost**.**

Table 1: Geometric parameters of steam-jet vacuum pump

Geometric parameters	Value (mm)
Diameter of nozzle throat	2
Diameter of nozzle inlet section	7.75
Expand angle of nozzle	10°
Diameter of mixing chamber inlet section	24
Diameter of throat	19
Length of mixing chamber	130
Length of throat	95
Length of diffuser	180

Table 2: Properties of steam used in the simulation

Properties	Value
Dynamic viscosity, μ	1.34×10^{-5} kg m^{-1} s^{-1}
Thermal conductivity, K	0.0261 Wm^{-1} K^{-1}
Specific heat capacity, C_p	2014.00 J kg^{-1} K^{-1}
Molecular weight, M	18.01534 kg kmol^{-1}

The commercial CFD code ANSYS-Fluent 6.3 was employed as a platform for CFD simulation. Quadrilateral structure meshes were used in 2D axis symmetric model, and the dense meshes are preset at the mixing zone as shown in Fig. 2(a). Fig. 2(b) shows the adapted meshes where it is possible to guess the location of high velocity gradient in present study. Boundary conditions are two pressure inlet boundaries and one pressure outlet boundary.

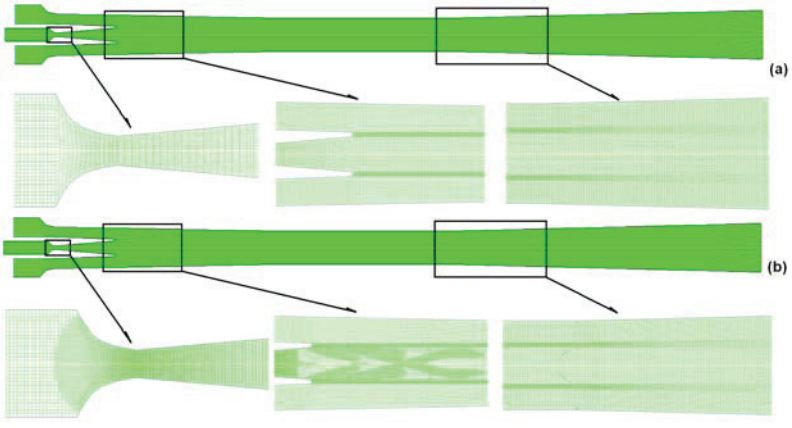

Fig. 2: The structure of steam-jet pump and grid of CFD calculating domain: (a) dense meshes (b) adapted meshes

The governing equations were solved by a finite-volume approach; the convection terms were discretized with second-order upwind scheme and a central difference discretization was used in the diffusion terms. The discretized system was solved by Gauss Seidel method. The couple-implicit solver was chosen to solve the governing equations, enhanced wall functions were used to describe the near-wall flow. Computations are stopped when residues fall below 10^{-6}, the mass imbalance (difference between mass flow on inlet and outlet boundaries) falls below 10^{-7} and the solution is no longer changing.

4. Results and discussions

4.1. Validation of CFD simulations and evaluation of turbulence models

The static pressure of simulation results obtained by the concerned turbulence models and the experimental data from Sriveerakul [15] along steam-jet pump wall under specific operating conditions (P_p=198483 Pa, P_s=1227.9 Pa, T_p=393 K, T_s=283 K, P_b=3000 Pa) is shown in Fig. 3. It is clear that the RSM model represents the static pressure profile near the wall region most closely, followed by k-omega-SST model. This close agreement also validated the mathematic models. However, neither k-epsilon based models nor RSM model could give correct simulation results and describe the pressure curve exactly within the range of mixing chamber. The discrepancy between the experimental value and numerical value may due to the spontaneous condensation phenomenon happened in supersonic flow [17]. Since the results accuracy of k-omega-SST model is almost the same with RSM, and the CPU cost is relatively low, the k-omega-SST model was chosen as the tool model, and the follow simulation results were obtained based on the present model and numerical strategy.

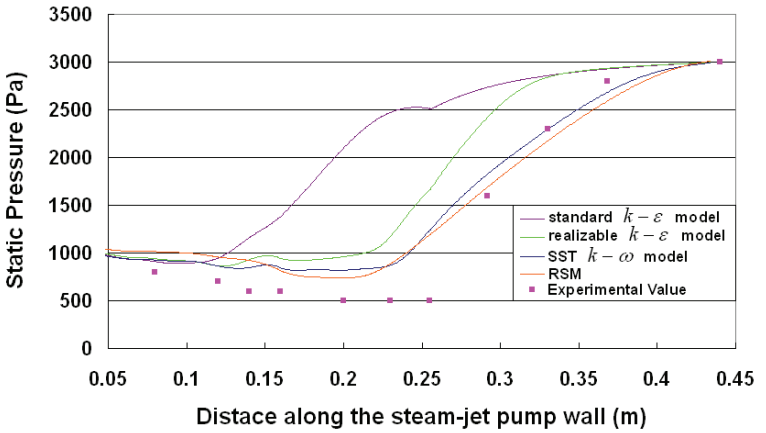

Fig. 3: Static pressure profiles along the steam-jet pump wall

4.2. Determination of shock-mixing layer

In this part, the location and shape of the key flow structure in a steam-jet pump, shock-mixing layer, were finalized by comparing the Mach values extracted from different sections in the pump. With the help of the powerful visualization function provided in ANSYS-Fluent package, this purpose could be achieved feasibly and conveniently.

Based on the simulation results, contours lines of Mach number (Fig. 4 (a)), under the specific operating condition (P_p=270018 Pa, P_s=1227.9 Pa, T_p=403 K, T_s=283 K, P_b=3000 Pa), a section of arbitrary in the mixing chamber (x=75 mm) was chosen as the reference position. The Mach values profile on the reference position along the radial direction (Fig.4 (b)) was compared with the Mach values distribution along the axis of the pump (Fig.4 (c)), it is clear that the Mach value M_A at the maximum gradient point in Fig.4 (b) equals with the Mach value M_B at the shocking position in Fig.4 (c), $M_A = M_B$. According the classical jet pump theory, the shock-mixing layer lies

between the primary steam and the secondary steam, so the maximum velocity gradient is on the shock-mixing layer. It means that the Mach number on the shock-mixing layer equals with the Mach number on the shocking position, based on this conclusion, the location of the shock-mixing layer could be found easily, and the understanding of flow structure in the steam-jet vacuum pump became more clearly.

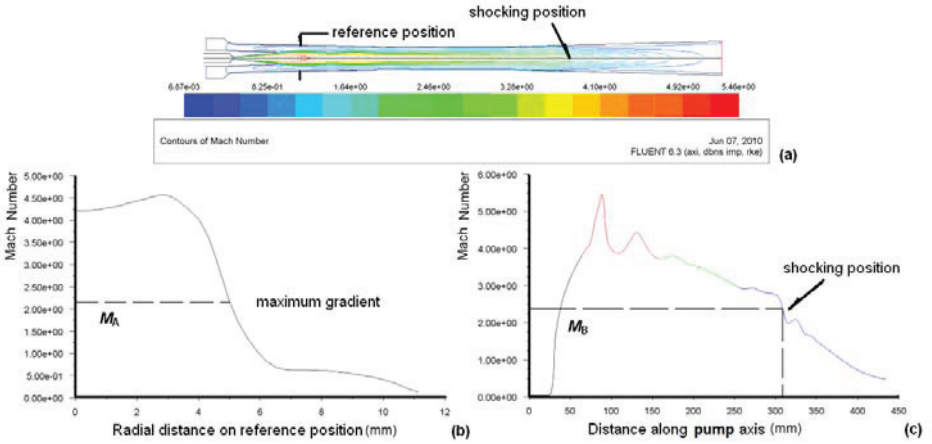

Fig. 4: Position determination of shock-mixing layer

Fig.5 represents the location and the shape of the shock-mixing layer inside the pump working under different back pressures (Fig 5 (a) for P_b=3000 Pa, Fig 5 (b) for P_b=3500 Pa, Fig 5 (c) for P_b=4000 Pa), it is clear that the secondary steam does not mix with the primary steam after inducing into the mixing chamber of the steam-jet vacuum pump, actually, they maintain their independence till the shocking position instead. After the shock happens, the shock-mixing layer disappear, the two fluid in the pump begin to mix with each other and discharge to the next stage with almost the same state. It is also observed that, with the back pressure increasing from 3000 Pa to 4000 Pa, the profile of the shock-mixing layer shrinks towards upstream, and the two steams redistribute their influence region at the same time.

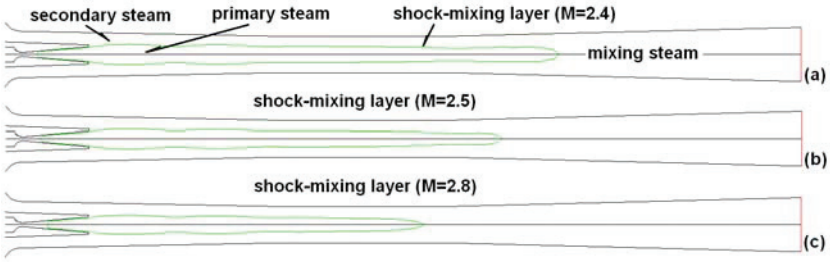

Fig. 5: The position of shock-mixing layer and the distribution of working fluid in the steam-jet pump

4.3 Analysis of the flow duct for the secondary steam

Based on the location and the shape of the shock-mixing layer, it is obviously that the flow duct for the secondary steam measures up with characteristics of general converging-diverging nozzle which is also composed of converging duct, throat, and diverging duct (Fig. 6 for P_b=3000 Pa). The only difference between them is that the inner wall is acted by the periphery of the primary steam jet core which is a motive wall and provides most of the energy to accelerate the secondary steam. Most of the entrained secondary steam reaches sonic velocity at the indicated section in Fig. 6, certain amount of them move faster than the sonic value when it flows close to the shock-mixing layer, but slower when it move close to the wall boundary layer. Meanwhile, the intensity of the primary steam jet core reduces and runs at a lower supersonic speed resulting in a relatively smooth jet core. Therefore, the annulus tunnel between this relatively smooth part of the shock-mixing layer and the wall of the throat of the steam-

jet pump after the indicated section where most of the secondary steam reaches sonic speed is acting as the throat of the duct for the secondary steam, and the choke area or effective area [5] of the secondary steam can be estimated at anywhere within the throat of the duct for the secondary steam obviously.

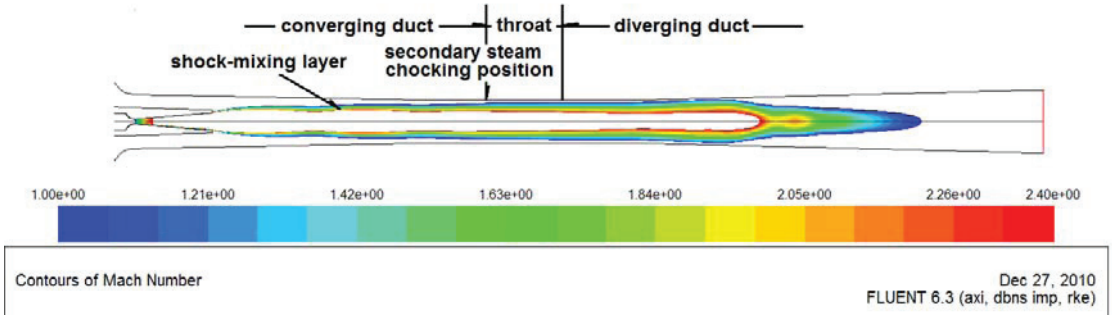

Fig. 6 The structure of the hypothetical duct for the secondary steam

4.4 Effect of operating conditions

The investigation of the effect of operating conditions on shock-mixing layer was carried out over a variety of back pressure in this paper. During the simulation, the back pressure ranged from 3000 Pa to 5500 Pa, while the other operating parameters were kept constant (P_p=270018 Pa, P_s=1227.9 Pa, T_p=403 K, T_s=283 K). It is already known that the operating modes of steam-jet pump could be divided into double choking, single choking and reverse flow modes by changing back pressure in the downstream [18]. This phenomenon is described in Fig.7 according the simulation results. When the back pressure keeps below the critical back pressure ($P_b \leqslant P_b^*$), the pump is working under double choking mode, its entrainment ratio remains constant and stable. When the back pressure rises above the critical back pressure and still below the break down pressure ($P_b^* < P_b \leqslant P_{b0}$), the entrainment ratio decreases sharply. This sudden drop indicates the steam-jet pump operates in single choking mode. After that, if the back pressure value keeps growing ($P_b > P_{b0}$), the flow structure in the pump was broken down totally and the pump could not work any more as already discussed in our previous work [16]. The understanding of effective area [5] and throat of the flow duct for the secondary steam could give a more reasonable explanation over this phenomenon from the internal flow structure aspect (Fig 8).

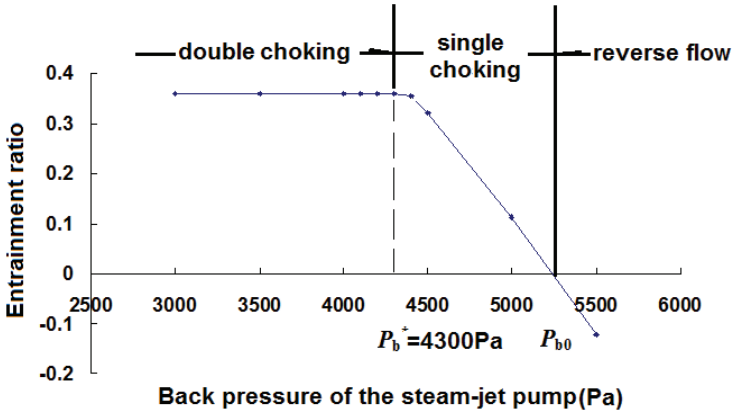

Fig. 7 Operational modes of steam-jet pump

Fig. 8 represents the shape of the shock-mixing layer and the secondary steam region which flows at a supersonic speed over a variety of back pressure. After knowing the characteristics of the flow duct for the secondary steam, based on the shape of the shock-mixing layer and the flowing state of the secondary steam, the length of the throat for this duct and its effective area size could be located and evaluated conveniently.

It is described that the secondary steam becomes choking at the same position and the length of the throat for the secondary steam flow duct shrinks towards upstream when the value of the back pressure increases but still keeps below the critical back pressure (P_b^*=4300 Pa) or within the double choking region. Moreover, the shape of the shock-mixing layer and the supersonic region of the secondary steam in front of the throat for the secondary steam flow duct are shown unchanged. That means before the choking position for the secondary steam, the flow structure remains constant and independent from the downstream conditions. That is why the entrainment ratio keeps constant when the pump is working under double choking mode.

When the back pressure is increased over the critical back pressure (P_b^*=4300 Pa), as it is shown in Fig. 8, the shock-mixing layer is compressed into the mixing chamber of the steam-jet pump, and the flow duct for the secondary steam lost its throat and it is no longer suitable for accelerating the induced steam any more, hence, the secondary steam can not get enough energy from the primary steam to speed up itself. Once the secondary steam is not choking, the stable entrainment process is disturbed, the entrainment ratio decreases sharply as a result.

It is also demonstrated that the length of the throat of the flow duct for the secondary steam is a useful criterion for evaluating the capacity of back pressure endurance for the pump. For a given operating conditions, if the secondary steam flow duct has a longer throat, that means the pump can work under a wide range of back pressure changing without performance decrease.

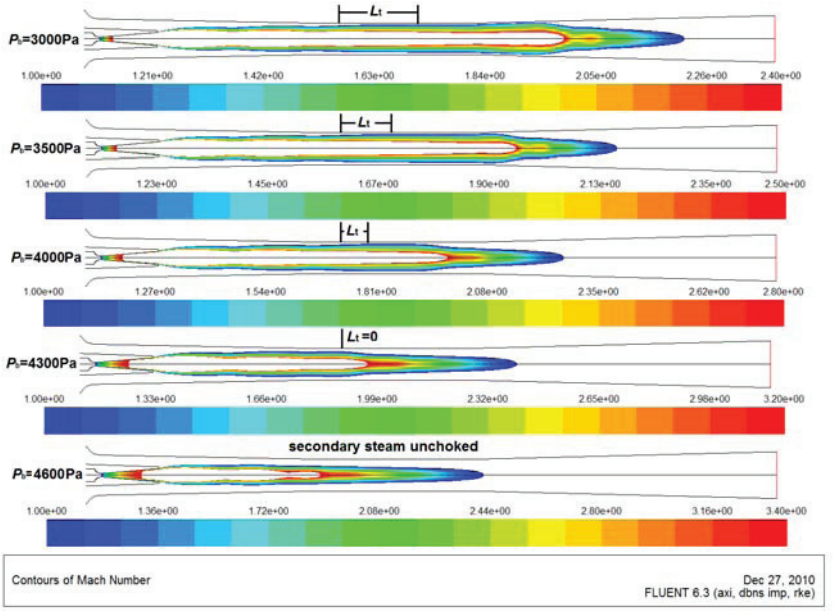

Fig. 8 The length of the throat for the secondary steam duct on respect of different back pressure

5. Conclusions

(1) CFD approach has been used successfully to simulate and capture the transonic flow structure in steam-jet pump, and can be used as a research tool to analyze and understand the shock-mixing layer which can provide a good understanding of local flow structure of the steam-jet vacuum pump.

(2) It has been shown that the k-omega-SST model is the best suited model to predict the pressure recovery profile along the pump wall. However, all models concerned in this paper seem to fail in predicting pressure near the wall within the range of mixing chamber. This discrepancy may due to the spontaneous

condensation phenomenon happened in supersonic flow which has been researched in many other studies and experiments.

(3) The method introduced in present study is reasonable and feasible; it can be used in locating the shock-mixing layer and understanding its feature in the whole flow field of the steam-jet pump.

(4) Based on the work of shock-mixing layer determination, a detailed analysis about the flow duct for the secondary steam is provided. It is shown that the throat for the secondary steam flow duct plays a crucial role in maintaining a stable pump operation state and the throat length reflects the back pressure endurance for the pump.

(5) Further studies should be taken based on this work, such as the effective area changing for the secondary steam on the respect of different operating conditions and pump geometries. That will be helpful for understanding the flow mechanism of the steam-jet pump and improve its performance eventually.

Acknowledgment

The financial support provided by the foundation of international cooperation project (ID7440015), the doctoral foundation for returning-back scholar of Northeastern University (ID18504032) and the Australian Research Council (ID DP0877734) is gratefully acknowledged.

References

[1] M.C. Huang, S.L. Chen, An experimental investigation of ejector performance characteristics in a jet refrigeration system. Journal of the Chinese Institute of Chemical Engineering E 1996; 27(2): 91-100.

[2] I.W. Eames, S. Aphnonratana. Research on heat operated heat pumps and refrigerators. Journal of the Institute of Energy 1993; 66: 29-39.

[3] Kanjanapon Chunnanond, Satha Aphornratana. Ejectors: Applications in refrigeration technology. Renewable and Sustainable Energy Reviews 2004; 8: 129-155.

[4] J.H. Keenan, E.P. Neumann. A simple air ejector. ASME Journal of Applied Mechanics 1942; 64: 75-82.

[5] J.T. Munday, D.F. Bagster. A new theory applied to steam jet refrigeration. Industrial & Engineering Chemistry Process Design and Development 1977; 16: 442-449.

[6] I.W. Eames, S. Aphornratana, H. Haider. A theoretical and experimental study of a small-scale steam jet refrigerator. International Journal of Refrigeration 1995; 18(6): 378-386.

[7] P. Desevaux, J. P. Prenel, G. Hostache. Flow visualization methods for investigating an induced flow ejector. Flow Visualization Image Process 1995; 2: 61-74.

[8] Y. Bartosiewicz, Zine Aidoun, P. Desevaux, Yves Mercadier. Numerical and experimental investigations on supersonic ejectors. International Journal of Heat and Fluid Flow 2005; 26: 56-70.

[9] Bartosiewicz Y, Aidoun Z, Desevaux P, Mercadier Y. Numerical and experimental investigations on supersonic ejectors. International Journal of Heat and Fluid Flow 2005; 26: 56-70.

[10] Hemidi A, Henry F, Leclaire S, Seynhaeve J, Bartosiewicz Y. CFD analysis of a supersonic air ejector. Part 1: experimental validation of single-phase and two-phase operation. Applied Thermal Engineering 2009; 29: 1523-1531.

[11] Ouzzane M, Aidoun Z. Model development and numerical procedure for detailed ejector analysis and design. *Applied Thermal Engineering* 2003; 23: 2337-2351.

[12] Y. Bartosiewicz, Y. Mercadier, P. Proulx. Numerical investigations on dynamics and heat transfer in a turbulent under-expanded jet. *AIAA Journal* 2002; 40 (11), 2257-2265.

[13] ANSYS INC. ANSYS-Fluent Theory guide.

[14] F. R. Menter. Two-equation eddy-viscosity turbulence models for engineering applications. *AIAA Journal* 1994; 32(8):1598-1605.

[15] Sriveerakul T, Aphormratana S, Chunnanond K. Performance prediction of steam ejector using computational fluid dynamics: part 1. Validation of the CFD results. *International Journal of Thermal Sciences* 2007; 46: 812-822.

[16] Xiao-Dong Wang, Jing-Liang Dong. Numerical study on the performances of steam-jet vacuum pump at different operating conditions. *Vacuum* 2010; 84: 1341-1346.

[17] Ishazaki K, Ikohagi T, and Daiguji H. A high-resolution numerical method for transonic non-equilibrium condensation flows through a steam turbine cascade. *In Proceedings of the 6th International Symposium on Computational Fluid Dynamics* 1995; 1: 479-484.

[18] H. Jeong, T. Utomo, M. Ji, Y. Lee, G. Lee, H. Chung. CFD analysis of flow phenomena inside thermo vapor compressor influenced by operating conditions and converging duct angles. *Journal of Mechanical Science and Technology* 2009; 23: 2366-2375